Materials Letters 358 (2024) 135877

Contents lists available at ScienceDirect

Materials Letters

journal homepage: www.elsevier.com/locate/matlet

Graphene-wrapped Fe_2TiO_5 nanoparticles with enhanced performance as lithium-ion battery anode

Fei Xie [a,1], Meng Sun [a,1], Xiaoli Sheng [a], Qingye Zhang [a], Zhibin Ling [a], Shujin Hao [a], Feiyu Diao [b,*], Yiqian Wang [a,*]

[a] College of Physics, Qingdao University, No. 308 Ningxia Road, Qingdao 266071, People's Republic of China
[b] Industrial Research Institute of Nonwovens & Technical Textiles, Shandong Center for Engineered Nonwovens, College of Textiles & Clothing, Qingdao University, No. 308 Ningxia Road, Qingdao 266017, People's Republic of China

ARTICLE INFO

Keywords:
Fe_2TiO_5 nanoparticles
Graphene
Anode material
Lithium-ion batteries
Electrochemical performance

ABSTRACT

Iron-titanium bimetallic oxide, Fe_2TiO_5 (FTO), is anticipated to exhibit superior electrochemical properties due to its high theoretical capacity. However, the practical large-scale utilization of FTO is severely hindered by its substantial capacity fading and subpar cycling performance. In this work, we propose a strategy to improve the electrochemical properties of FTO by carbon coating. To implement this strategy, we synthesize FTO nanoparticles (FTO NPs) coated with reduced graphene oxide (rGO) by a solvothermal method. When used as anode materials in lithium-ion batteries, FTO/rGO composite demonstrates a higher specific capacity (498.2 mAh g^{-1} after 100 cycles) than pristine FTO NPs, which is ascribed to the addition of rGO. The rGO with excellent conductivity facilitates efficient electron and ion transportation, and the composite structure of FTO NPs wrapped with rGO provides buffer space to alleviate the volume expansion during the charge/discharge process.

1. Introduction

Fe_2TiO_5 (FTO) has attracted much attention in lithium-ion batteries (LIBs) due to its high theoretical capacity and environmental friendliness [1]. However, the substantial capacity fading and inferior cycling performance are common problems for transition metal oxides [2,3]. To achieve better electrochemical performance, researchers have devoted great efforts to combining transition metal oxides with other materials that can alleviate the volume changes, *i.e.*, carbon [4]. In this case, carbon coating can enhance the cycling stability because it can inhibit the aggregation of FTO nanoparticles (FTO NPs) [5]. Therefore, the fabrication of a hybrid structure comprising FTO and graphene presents a promising strategy for the development of high-performance anode materials in LIBs.

In this work, we report on a two-step solvothermal method for the synthesis of hybrid FTO NPs decorated with reduced graphene oxide (rGO). The resulting FTO NPs/rGO composites exhibit a superior electrochemical performance compared to pristine FTO NPs when employed as anode materials in LIBs. This enhancement in electrochemical performance can be attributed to the introduction of rGO, which alleviates the volume expansion and aggregation of FTO NPs during electrochemical cycle.

2. Experimental

FTO NPs were produced through a solvothermal method and subsequent annealing in air. Then FTO NPs and rGO were mixed to prepare FTO NPs/rGO composites through a solvothermal method and subsequent annealing in argon. Their morphology, structure and microstructure were characterized by different techniques and their electrochemical performances were investigated. Experimental details are provided in the supplementary information.

3. Results and discussion

Fig. 1(a) shows the X-ray diffraction (XRD) patterns of FTO NPs and FTO NPs/rGO composites, revealing sharp diffraction peaks corresponding to specific crystal planes of orthorhombic FTO phase (JCPDS no.: 41–1432). After careful examinations, it is found that FTO NPs/rGO composites show diffraction peaks with lower intensities compared to

* Corresponding authors.
E-mail addresses: fydiao@qdu.edu.cn (F. Diao), yqwang@qdu.edu.cn (Y. Wang).
[1] These authors contributed to this work equally.

https://doi.org/10.1016/j.matlet.2024.135877
Received 4 October 2023; Received in revised form 19 December 2023; Accepted 2 January 2024
Available online 3 January 2024
0167-577X/© 2024 Elsevier B.V. All rights reserved.

FTO NPs, which is attributed to the addition of rGO. Further evidence is presented in the Raman spectrum of FTO NPs/rGO composites, as shown in Fig. 1(b). The Raman spectrum of rGO in Fig. 1(b) exhibits characteristic peaks at wavenumbers 1335 cm^{-1} (D band) and 1580 cm^{-1} (G band). These peaks are also observed in the Raman spectrum of FTO NPs/rGO, confirming the presence of rGO in the composite. The intensity ratios of D and G bands of rGO and FTO NPs/rGO are 1.016 and 1.007, indicating that the graphitization degree remains unchanged after wrapping with rGO. Both FTO NPs and FTO NPs/rGO composites show similar characteristic Raman peaks of FTO without significant peak position changes, indicating that FTO NPs are not bonded to rGO. This suggests that the FTO NPs/rGO composites are composed of separated phases of FTO and rGO. The content of rGO in the composites is determined to be 10 wt% from Fig. S3.

Fig. 2(a) and (d) show typical scanning electron microscope (SEM) images of FTO NPs and FTO NPs/rGO composites, respectively. The FTO NPs and FTO NPs/rGO composites have uniform sizes, with an average diameter of 18.8 nm and 20.3 nm, respectively. Thus, it can be deduced that the size of FTO NPs remains unchanged after rGO coating. SEM image in Fig. 2(d) reveals that FTO NPs are coated with flexible rGO layers. The incorporation of graphene enhances electron transfer and improves the electrical conductivity of the FTO NPs/rGO composites by formation of a conductive network. Fig. 2(b) and (c) show bright-field (BF) and high-resolution transmission electron microscopy (HRTEM) images of FTO NPs, respectively. In Fig. 2(b), FTO NPs have even size with an average size of 19.0 nm, consistent with our SEM observation. From Fig. 2(c), the lattice spacing is measured to be 3.48 Å, corresponding to the (1 0 1) crystal plane of FTO. Fig. 2(e) and (f) demonstrate the BF and HRTEM images of FTO NPs/rGO, respectively. In Fig. 2(e), it can be seen that FTO NPs are uniformly distributed on the rGO surface, where the layered arrangement of rGO is indicated by red arrows. From Fig. 2(f), we measure a lattice spacing of 4.90 Å, matching the (2 0 0) crystal plane of FTO.

To investigate the lithium storage capacity of FTO NPs and FTO NPs/rGO electrodes, half-cells were assembled and tested. Fig. 3(a) and (b) display the cyclic voltammetry (CV) curves of FTO NPs and FTO NPs/rGO electrodes during the first six charge–discharge cycles. As shown in Fig. 3(a), four distinct reduction peaks (1.8 V, 0.9 V, 0.5 V, 0.2 V) and one oxidation peak (1.5 V) are observed in the first CV curve. Overall, the CV curves of FTO NPs and FTO NPs/rGO electrodes demonstrate similar peak positions in both reduction and oxidation processes. However, the reduction peak at 0.9 V for FTO NPs/rGO is weaker than that for FTO NPs, which might be related to the reduced mass proportion of FTO in the composites. The electrochemical reactions of FTO during charge–discharge cycles are summarized using the following equations [6].

$$Fe_2TiO_5 + xLi^+ + xe^- \leftrightarrow Fe_2O_3 + Li_xTiO_2 \quad (1)$$

$$TiO_2 + xLi^+ + xe^- \leftrightarrow Li_xTiO_2 \quad (2)$$

$$Fe_2O_3 + 2Li^+ + 2e^- \leftrightarrow Li_2(Fe_2O_3) \quad (3)$$

$$Li_2(Fe_2O_3) + 4Li^+ + 4e^- \leftrightarrow 2Fe^0 + 3Li_2O \quad (4)$$

Fig. 3(c) displays the electrochemical cycling performance of FTO NPs (theoretical specific capacity: 783 mAh g^{-1}) and FTO NPs/rGO (theoretical specific capacity: 742 mAh g^{-1}) under a current density of 0.1 A g^{-1}. It is observed that the discharge capacity of FTO NPs electrode drops to 78.5 mAh g^{-1} after 100 cycles, suggesting that the structure of FTO has been damaged due to the large volume change of the electrode material during cycling. Compared to FTO NPs, FTO NPs/rGO electrode exhibits a higher capacity of 498.2 mAh g^{-1} after 100 cycles. The capacity is initially decreasing and then increasing with the cycle number, which is attributed to the irreversibility of some electrochemical reactions and the gradual activation of the active substance, respectively. As shown in Fig. 3(d), the average discharge capacities of FTO NPs/rGO electrode are 483.5, 326.9, 263.6, 214.2, and 155.5 mAh/g at 0.1, 0.2, 0.5, 1.0 and 2.0 A/g, respectively. Moreover, as the current density bounces back to 0.1 A/g, the reversible capacity of FTO NPs/rGO electrode still maintains 453.7 mAh/g, higher than that of FTO NPs (85.3 mAh/g). The enhanced electrochemical performance of FTO NPs/rGO electrode is attributed to the introduction of rGO into the composite structure.

As observed from Fig. 4(a), the electrochemical impedance spectroscopy (EIS) spectra consist of semi-circles and inclined lines in high frequency and low frequency regions, respectively. In the high frequency region, the half-circle diameter of FTO NPs/rGO composites is clearly smaller than that of FTO NPs, suggesting that they possess lower contact and charge-transfer resistances [7]. The relationship between Z_{re} and $\omega^{-0.5}$ is displayed in Fig. 4(b). The diffusion coefficient of Li^+ (D_{Li}) is calculated using the following equation [8].

$$D_{Li} = \frac{R^2T^2}{2A^2n^4F^4C^2\sigma^2} \quad (5)$$

where the values of Faraday constant (F) and gas constant (R) are 96,485C mol^{-1} and 8.314 J K^{-1} mol^{-1}. The electrode area A is 1.54 × 10^{-4} m^2, T is 298.15 K, n is the number of the electrons per single molecule participating in the electron transfer reaction, and C represents the lithium-ion concentration of the electrode. Z_{re}, R_s, R_{ct} and ω denote the impedance, electrolyte resistance, charge-transfer resistance and frequency, respectively. D_{Li} values are calculated to be 4.3 × 10^{-18} and 1.8 × 10^{-17} cm^2 s^{-1} for FTO NPs and FTO NPs/rGO electrodes, respectively. The conductivity σ of the electrodes is expressed by the following equation [9], corresponding to the slope of the straight line in Fig. 4(b).

$$Z_{re} = R_s + R_{ct} + \sigma\omega^{-0.5} \quad (6)$$

The linear regressions in Fig. 4(b) give σ values of 59.9 and 29.6 Ω $s^{-0.5}$ for FTO NPs and FTO NPs/rGO electrodes, respectively.

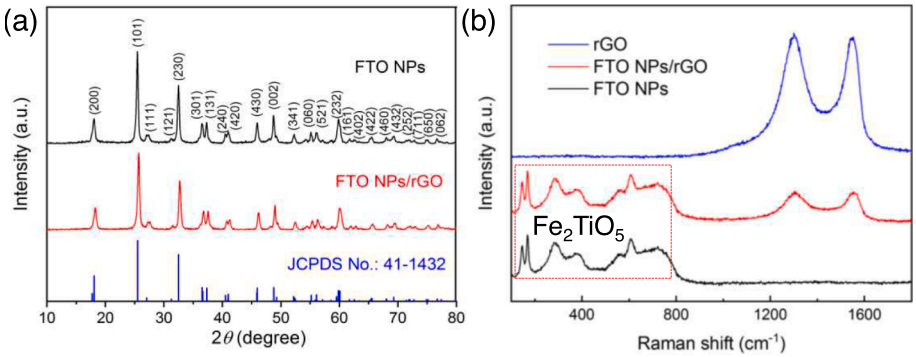

Fig. 1. (a) XRD patterns of the FTO NPs and FTO NPs/rGO composites. (b) Raman spectra of rGO, FTO NPs and FTO NPs/rGO composites.

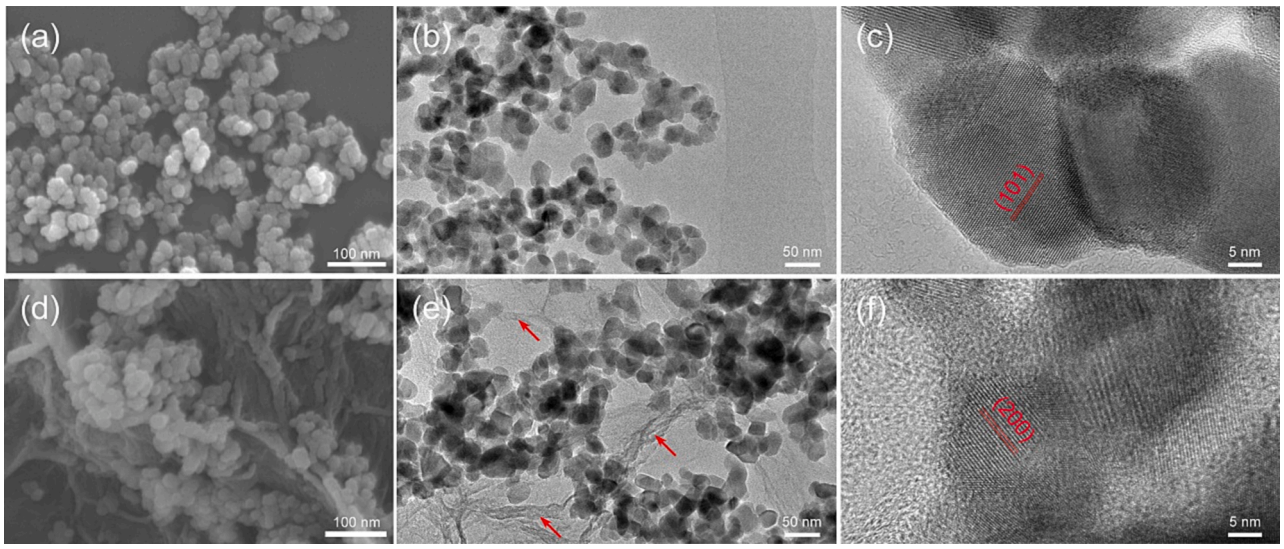

Fig. 2. Typical SEM image (a), BF TEM image (b) and HRTEM image (c) of FTO NPs; Typical SEM image (d), BF TEM image (e) and HRTEM image (f) of FTO NPs/rGO composites.

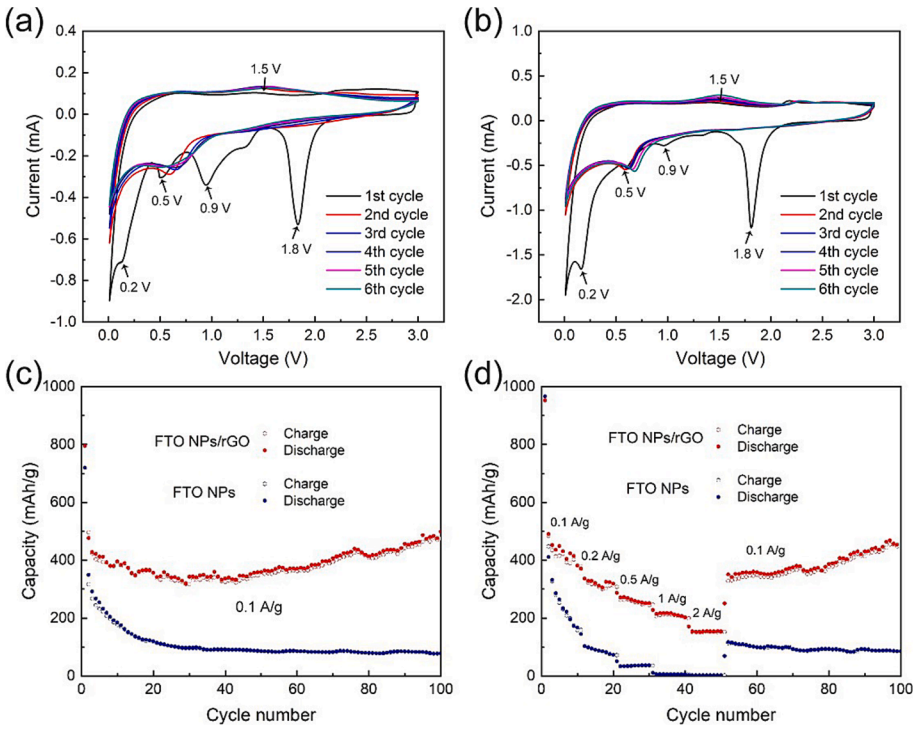

Fig. 3. CV curves of FTO NPs (a) and FTO NPs/rGO (b) obtained at 0.3 mV s^{-1}. (c) Cycling performance and (d) rate performance of FTO NPs and FTO NPs/rGO electrodes.

4. Conclusions

In summary, we propose a carbon coating strategy to enhance the electrochemical performances of FTO NPs. FTO NPs/rGO composite electrode displays excellent specific capacity (498.2 mAh g^{-1} after 100 cycles), higher than that of FTO NPs. Furthermore, it demonstrates superior rate performance compared to FTO NPs, owing to the presence of rGO. Besides, the large volume changes during charge and discharge can be buffered by carbon coating, thus promoting the cyclic stability of the electrode material. Our results suggest that the FTO NPs/rGO composites hold significant promise as high-performance anode materials for LIBs.

CRediT authorship contribution statement

Fei Xie: Data curation, Investigation, Writing – original draft. **Meng Sun:** Data curation, Investigation, Methodology. **Xiaoli Sheng:** Methodology. **Qingye Zhang:** Formal analysis, Resources. **Zhibin Ling:** Methodology, Resources. **Shujin Hao:** Resources. **Feiyu Diao:** Validation, Writing – review & editing. **Yiqian Wang:** Conceptualization, Funding acquisition, Project administration, Writing – review & editing.

Declaration of competing interest

The authors declare that they have no known competing financial

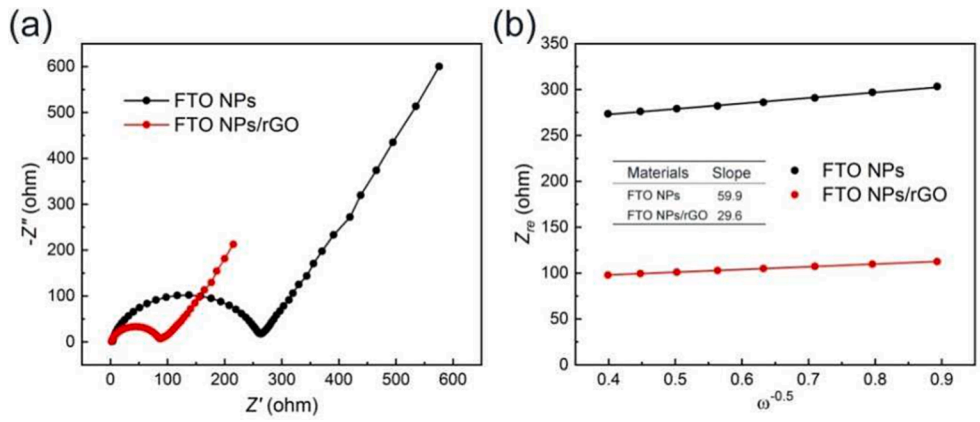

Fig. 4. (a) EIS plots of FTO NPs and FTO NPs/rGO electrodes. (b) Graph of Z_{re} plotted against $\omega^{-0.5}$.

interests or personal relationships that could have appeared to influence the work reported in this paper.

Data availability

Data will be made available on request.

Acknowledgements

The authors would like to thank the financial support from High-end foreign experts project of the Ministry of Science and Technology, China (Grant no.: G2022025015L, G2022025016L), the Shandong Province "Double-Hundred Talent Plan" (Grant No.: WST2018006), and the Top-notch Innovative Talent Program of Qingdao City, China (Grant no.: 13-CX-8). Y. Q. Wang would also like to thank the financial support from the Taishan Scholar Program of Shandong Province, China, Qingdao International Center of Semiconductor Photoelectric Nanomaterials. Thanks for helpful discussion with Professor Francois Schiettekatte from University of Montréal, Canada.

Appendix A. Supplementary data

Supplementary data to this article can be found online at https://doi.org/10.1016/j.matlet.2024.135877.

References

[1] H. Liu, Z. Li, H. Sun, Q. Lu, Energy Tech. 8 (2020) 2000215.
[2] S.C. Weng, S. Brahma, P.C. Huang, Y.C. Huang, Y.H. Lee, C.C. Chang, J.L. Huang, Appl. Surf. Sci. 505 (2020) 144629.
[3] Y.C. Huang, S. Brahma, C.C. Chang, J.L. Huang, J. Electrochem. Energy Convers. Storage 19 (2022) 011006.
[4] C.C. Hou, S. Brahma, S.C. Weng, C.C. Chang, J.L. Huang, J. Electrochem. Energy Convers. Storage 17 (2020) 031003.
[5] Y.L. Liu, C. Yan, G.G. Wang, F. Li, J.S. Huang Fu, B.W. Wu, H.Y. Zhang, J.C. Han, Nanotechnology 31 (2020) 265405.
[6] K.S. Lee, S. Park, W. Lee, Y.S. Yoon, ACS Appl. Mater. Interfaces 8 (2016) 2027–2034.
[7] A. Kim, H. Jung, J. Song, H.J. Kim, G. Jeong, H. Kim, A.C.S. Appl, Mater. Interfaces 11 (2019) 9054–9061.
[8] M. Sun, X. Sheng, S. Li, Z. Cui, T. Li, Q. Zhang, F. Xie, Y.Q. Wang, J. Alloy. Compd. 926 (2022) 166809.
[9] X. Sheng, T. Li, M. Sun, G. Liu, Q. Zhang, Z. Ling, S. Gao, F. Diao, J. Zhang, F. Rosei, Y.Q. Wang, Electrochim. Acta 407 (2022) 139892.